Entry Characteristics of a Half-Ogive Aeroshell at Earth

AE 8900 MS Special Problems Report
Space Systems Design Lab (SSDL)
Guggenheim School of Aerospace Engineering
Georgia Institute of Technology
Atlanta, GA

Author:
Robert M. Booher

Advisor:
Prof. Robert D. Braun

May 2, 2016

Entry Characteristics of a Half-Ogive Aeroshell at Earth

Robert M. Booher* and Robert D. Braun†
Georgia Institute of Technology, Atlanta, GA, 30332-1510, USA

Nomenclature

I_x	Roll inertia at mass center, kg-m^2
I_y	Pitch inertia at mass center, kg-m^2
I_z	Yaw inertia at mass center, kg-m^2
α	Aerodynamic angle of attack, deg
β	Aerodynamic roll angle, deg
θ	Angle of pitch, deg
q_∞	Freestream dynamic pressure, lbf/ft^2
S	Reference area, m^2
l	Reference length, m
V	Freestream velocity magnitude, m/s
C_m	Pitch moment coefficient
C_l	Lift force coefficient
C_d	Drag force coefficient
γ	Flight path angle, rad
s	Path length, m
g	Acceleration of gravity, m/s^2
m	Vehicle mass, kg
t	Time, s

I. Introduction

Current robotic exploration missions to Mars utilize variations of the Viking heritage sphere-cone to provide adequate entry deceleration prior to the descent and landing events. The drag area of these aeroshells is directly limited by the diameter of current launch vehicle payload fairings. The largest fairings currently available limit aeroshell diameter to approximately 4.5 meters. As landed payload mass has increased from small class landers such as Beagle 2 (30 kg)[1] to the Mars Science Laboratory's Curiosity rover (900 kg),[2] the combination of high mass and limited drag area has increased the entry ballistic coefficient nearing the limit of the current architecture's capability. Beyond robotic exploration, human exploration of the red planet and the delivery of supporting infrastructure and supplies is anticipated to require landed mass capabilities on the order of 10 to 50 metric tons,[3] well beyond the capabilities of the current heritage architecture. Multiple solutions to achieve higher landed mass at Mars have been proposed, most notably the development of inflatable decelerator technologies in the Low-Density Supersonic Decelerator (LDSD) project,[4] the Hypersonic Inflatable Aerodynamic Decelerator (HIAD) project,[5] and the Supersonic Inflatable Aerodynamic Decelerator (SIAD) project[6] have gained considerable traction and have achieved varying levels of proof of concept in Earth based testing. Attached inflatable decelerators seek to increase the drag area by augmenting the heritage Viking era architecture while remaining within the launch vehicle constrained

*Graduate Research Assistant, Daniel Guggenheim School of Aerospace Engineering, AIAA Student Member.
†David & Andrew Lewis Professor of Space Technology, Daniel Guggenheim School of Aerospace Engineering, AIAA Fellow.

diameter of 4.5 meters. This paper proposes a novel concept wherein one half of the launch vehicle payload fairing itself is used as the entry aeroshell at Mars. This dual purposing of the launch vehicle fairing improves mass to orbit performance, allows for significantly larger entry drag area, and affords the potential for significant lift modulation. Development of this architecture will require a series of Earth based test flights to improve confidence in the architecture, improve system models, and prove out design choices. The expected behavior of the aeroshell in these Earth based tests is the focus of this paper.

II. Flight Test Vehicle Model

Each launch vehicle provider in the United States uses their own unique payload fairing to protect customer payloads during ascent, but many of these fairings are variations on the ogive geometry. A visual comparison of various commercially available fairings is shown in figure 1. For this study, a generalized fairing half is approximated by a half ogive as depicted in figure 2 and it is assumed that the gross aerodynamic properties between the various fairing shapes available are comparable to this approximation. To evaluate the flight characteristics of the half-ogive, a model of the vehicle was constructed in a six degree-of-freedom trajectory simulation tool. Trajectories were initiated at entry interface and the entry conditions are listed in table 1. The mass properties and dimensions of the half ogive were developed to approximate those of current launch vehicle payload fairings and are also presented in table 1.

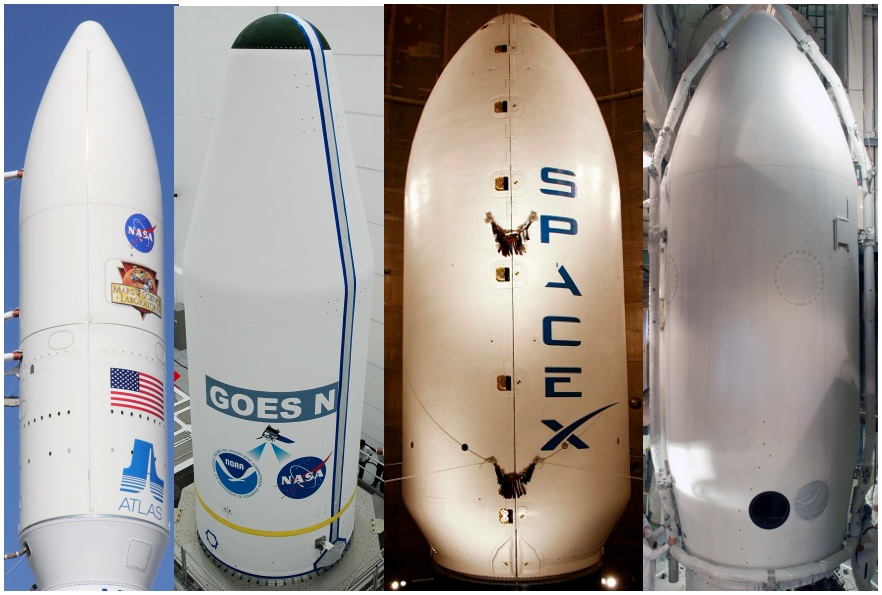

Credit left to right: Ken Kremer via Universe Today, NASA, SpaceX, NASA

Figure 1. Various commercially available launch vehicle payload fairings from United States based providers. From left to right: Atlas V (Lockheed Martin/ULA), Delta IV Medium (Boeing/ULA), Falcon 9 (SpaceX), Delta II 10C (Boeing/ULA)

Table 1. Simulation Configuration Parameters

Entry Conditions		
Altitude	100	km
Mach Number	9.45	
Earth Relative Velocity	2.6	km/s
Earth Relative Flight Path Angle	-18.7	deg
Total Angle of Attack	105	deg
Aerodynamic Roll Angle	0	deg
Vehicle Mass Properties		
Mass	1800	kg
Length (l)	12	m
Diameter (d)	5	m
I_x	7,000	kg-m^2
I_y	33,000	
I_z	37,000	
C.M. Location in Body Frame	$\left[4, 0, -1.2\right]$	m

A. Aerodynamics

Aerodynamics of the half-ogive shape were approximated by an inviscid CFD solver tool using a grid of angle of attack and aerodynamic roll angle combinations. The definition of these angles is shown in figure 2. Of particular interest are the vehicle's static stability derivatives as well as its lift to drag ratio. As shown in figure 3(a) and 3(b), the vehicle is statically stable in both total angle of attack and aerodynamic roll as specified by the restoring moment near the trim condition. The vehicle's trim angle of attack is approximately 105 degrees in supersonic flight and 95 degrees in subsonic flight for the center of gravity location specified. Though the entry trajectories presented in this study achieve a Mach number as high as 10, CFD results at these high Mach numbers were nearly identical to the Mach 4 result. Therefore the Mach 4 properties are also used for all higher Mach numbers.

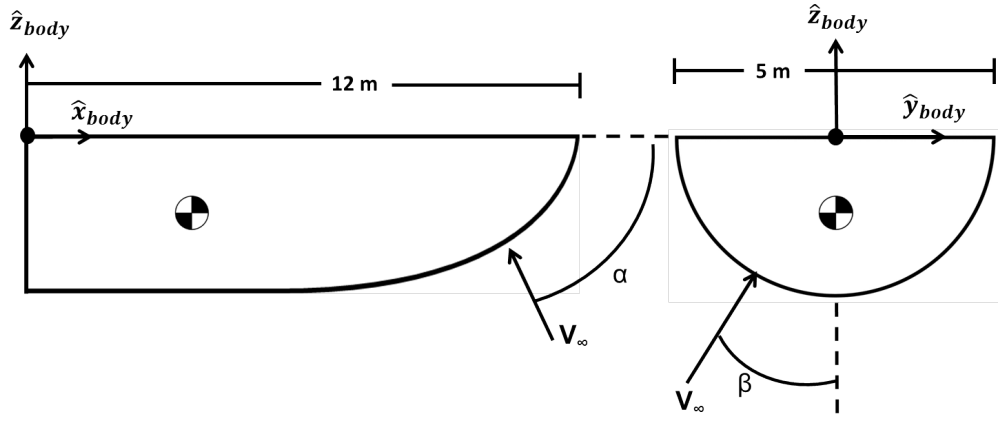

Figure 2. Angle of attack and aerodynamic roll angles are defined positive as shown. The body coordinate system origin is located along the vehicle centerline and lies in the plane of separation with the other fairing half.

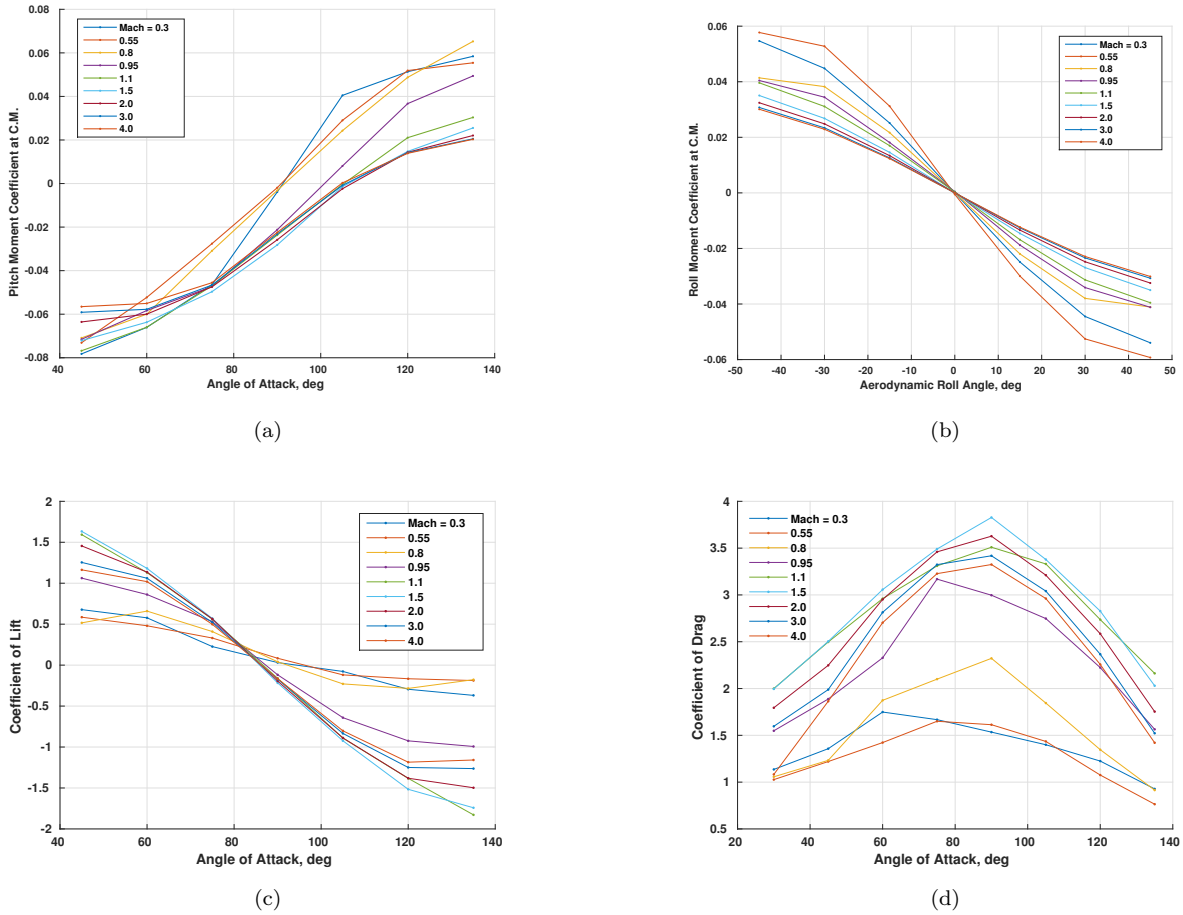

Figure 3. Important aerodynamic moment and force coefficients for the center of mass specified in table 1.

III. Results

A. Supersonic Flight Characteristics

Simulations of the vehicle predict extremely benign entry environments in terms of aerothermal heating, dynamic pressure and decceleration as shown in figure 4 and figure 6. The benign environment is a direct result of the vehicle's low ballistic coefficient. The mass estimate for this study assumes a minimal payload consisting only of the mass required to instrument the vehicle and record data. It is important to note that on operational flights of the half-ogive aeroshell, increasing the vehicle mass with the addition of mission payloads will significantly change the conditions seen during entry phase of flight.

B. Tolerance to Entry Attitude Error

To determine the vehicle's tolerance to entry attitude error, the entry attitude was dispersed from 45 to 135 degrees in total angle of attack while holding all other entry conditions constant. The results of each case is shown in figure 5. Even at these extreme entry attitude errors, the vehicle is shown to be resilient and seeks its trim condition. This is due to a combination of stable static aerodynamics as well as the vehicle's very low ballistic coefficient. The low inertia relative to the very large drag area allows the vehicle to more easily right itself in the low dynamic pressure environment at the onset of the entry event. This could allow for flight tests to employ relatively simple and low-cost navigation and attitude control systems.

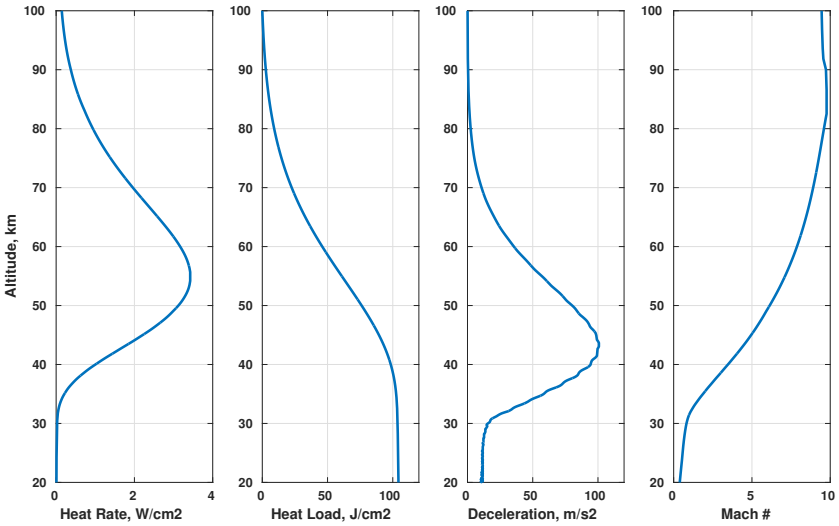

Figure 4. Supersonic entry conditions are relatively benign for the low system mass used in this study. Heat rate was calculated using the Chapman heating approximation with a nose radius equal to half the aeroshell diameter.

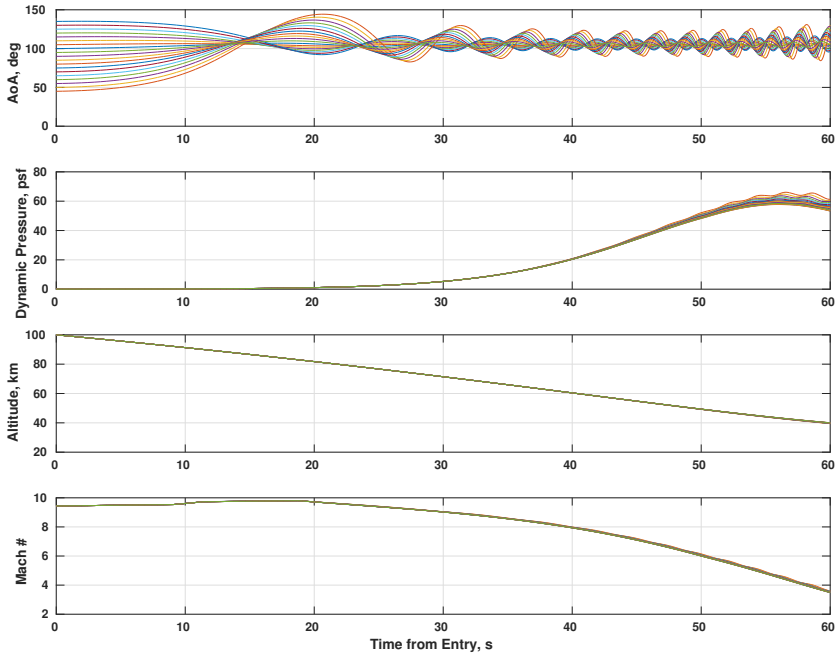

Figure 5. Dispersed entry angles-of-attack return to the supersonic trim condition in simulation.

C. Low-Speed Dynamic Instability

Aerodynamics of the half-ogive show that the aeroshell has static stability at its trim angle of attack and aerodynamic roll angle. If successfully positioned near its trim attitude at entry interface, a first order

analysis predicts the vehicle would remain stable barring any large disturbances. However, using only the static aerodynamic database generated with an inviscid CFD solver tool, 6-DOF entry trajectory simulations of the vehicle predict a dynamic and diverging pitch instability. An example trajectory showing this behavior is presented in figure 6, but virtually all simulations analyzed for this study yielded the same result.

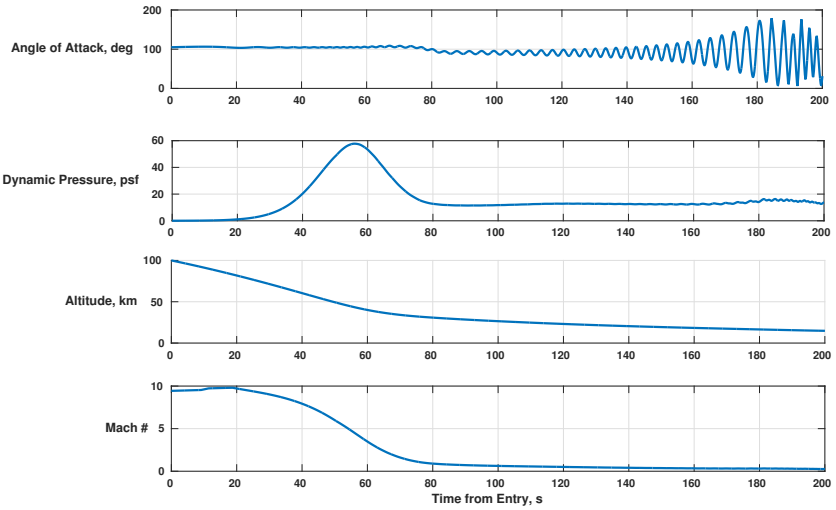

Figure 6. Simulations of the vehicle predict a divergence from the trim attitude leading to tumbling late in the entry event.

The source of this instability is of particular interest as it can provide insight into possible mitigation techniques. In this example and in all other cases analyzed, the divergence of the angle of attack to eventual tumbling of the vehicle is gradual and the vehicle tumbles well into the subsonic portion of the trajectory. Moreover, test cases utilizing simplified constant aerodynamics across all Mach numbers show the same behavior. Therefore the common culprit of significant transonic disturbances can be discarded. The angle of attack continues to diverge into the terminal descent portion of the trajectory when dynamic pressure is roughly constant, so the oscillation amplitude growth cannot be attributed to decreasing dynamic pressure. These simulations were also generated using an inviscid CFD database, so complex flow/aeroshell interactions will not be captured. Karatekin[7, 2.1.4] presents a candidate source of the instability as the angle of attack derivative of the lift vector. A thorough derivation of the governing equation of motion can be found in Ref. 7, but for this report, a brief overview is sufficient. The exact planar equation of motion for vehicle rotation in planetary entry is shown in Eq. (1).

$$I_y\ddot{\theta} = C_m q_\infty Sl + C_{m_q} q_\infty Sl\frac{l\dot{\theta}}{V} + C_{m_{\dot{\alpha}}} q_\infty Sl\frac{l\dot{\alpha}}{V} \tag{1}$$

Where

$$C_{m_q} = \frac{\partial C_m}{\partial\frac{\dot{\theta}l}{V}}, \quad C_{m_{\dot{\alpha}}} = \frac{\partial C_m}{\partial\frac{\dot{\alpha}l}{V}} \tag{2}$$

Using the relationship $\theta = \alpha - \gamma$, Eq. (1) can be written as:

$$\ddot{\alpha} - \ddot{\gamma} = \frac{q_\infty Sl}{I_y}\left[C_m + (C_{m_q} + C_{m_{\dot{\alpha}}})\frac{l\dot{\theta}}{V} + C_{m_q}\frac{l\dot{\gamma}}{V}\right] \tag{3}$$

The final form shown in Eq. (4) can be reached by using an exponential atmosphere model, changing the independent variable from time to path length (s) using Eq. (5), and neglecting small terms.

$$\frac{\partial^2\alpha}{\partial s^2} - \frac{\rho S}{2m}\left[C_d - \frac{gm}{q_\infty S}sin\gamma - \frac{\partial C_l}{\partial\alpha} + (C_{m_q} + C_{m_{\dot{\alpha}}})\frac{l^2 m}{I_y}\right]\frac{\partial\alpha}{\partial s} - \frac{\rho Sl}{I_y}C_m = 0 \tag{4}$$

$$\frac{\partial \alpha}{\partial t} = V\frac{\partial \alpha}{\partial s} \qquad \frac{\partial^2 \alpha}{\partial t^2} = V^2\frac{\partial^2 \alpha}{\partial s^2} + \frac{\partial V}{\partial t}\frac{\partial \alpha}{\partial s} \tag{5}$$

As mentioned above and seen in figure 6, the diverging oscillations become significant in the terminal descent portion of the trajectory when the flight path angle is very steep and the dynamic pressure is constant. For terminal descent, Karatekin presents a simplified form shown in Eq.(6) by taking into account assumptions of constant velocity, constant drag coefficient and constant dynamic pressure, all well justified when the vehicle is in terminal descent.

$$\frac{\partial^2 \alpha}{\partial s^2} - \frac{\rho S}{2m}\left[-\frac{\partial C_l}{\partial \alpha} + (C_{m_q} + C_{m_{\dot{\alpha}}})\frac{l^2 m}{I_y}\right]\frac{\partial \alpha}{\partial s} - \frac{\rho S l}{I_y}C_m = 0 \tag{6}$$

Departing from Karatekin with further simplifications, by neglecting C_{m_q} and $C_{m_{\dot{\alpha}}}$ because they are not modeled in the inviscid aerodynamic database, and by using the definition of dynamic pressure $q_\infty = \frac{1}{2}\rho V^2$, the equation of motion can be further reduced to the form shown in Eq.(7).

$$\frac{\partial^2 \alpha}{\partial s^2} - \frac{q_\infty S}{mV^2}\frac{-\partial C_l}{\partial \alpha}\frac{\partial \alpha}{\partial s} - \frac{2q_\infty S l}{I_y V^2}C_m = 0 \tag{7}$$

If a steady-state condition is assumed so that $\alpha = \alpha_0 + \Delta\alpha$, we can rewrite Eq.(7) as:

$$\frac{\partial^2 \alpha}{\partial s^2} + \frac{q_\infty S}{mV^2}\frac{\partial C_l}{\partial \alpha}\frac{\partial \alpha}{\partial s} - \frac{2q_\infty S l}{I_y V^2}\frac{\partial C_m}{\partial \alpha}\Delta\alpha = 0 \tag{8}$$

Representing the pitch axis equation of motion in this form clearly shows the dependence of both static and dynamic stability on the angle of attack derivatives of the pitch moment coefficient and the lift coefficient, respectively. The $\Delta\alpha$ term represents the static stability of the vehicle and therefore depends on the angle of attack derivative of the pitch moment coefficient. As shown previously, $\frac{\partial C_{My}}{\partial \alpha}$ is negative, resulting in an overall positive α term, so the vehicle is statically stable. The $\frac{\partial \alpha}{\partial s}$ term captures the dynamic stability of the vehicle. Eq.(8) can be used to obtain the dynamic stability criterion in terminal descent shown in Eq.(9). Figure 3(c) shows the lift coefficient as a function of angle of attack. The slope of this line is negative for all Mach numbers, so $\frac{\partial C_l}{\partial \alpha}$ is negative and therefore the dynamic stability criterion is not satisfied. The angle of attack oscillations will grow over time at a rate dependent on the magnitude of the overall $\frac{\partial \alpha}{\partial s}$ and $\Delta\alpha$ terms.

$$\frac{q_\infty S}{mV^2}\frac{\partial C_l}{\partial \alpha} > 0 \tag{9}$$

The overall static and dynamic terms across the trajectory are shown in figure 7. Though the system becomes more stiff as it decelerates to terminal descent, the dynamic term grows more negative from a near zero initial condition.The above evidence confirms that the pitch instability observed in simulation is a result of the dynamic instability derived above.

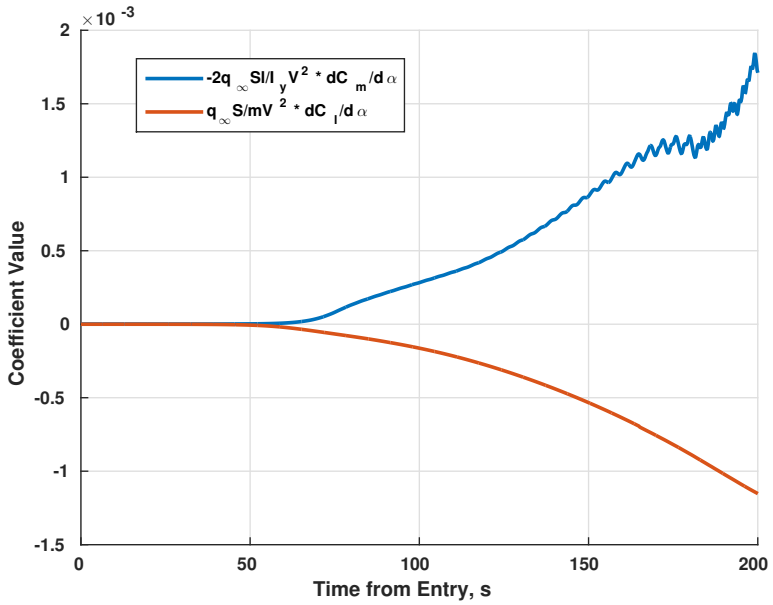

Figure 7. Stability terms across the trajectory show the system becomes less stable in terminal descent.

IV. Pitch Instability Mitigation

Mitigation of the divergent pitch behavior will be important for any Earth based test flight that aims to gather data in low velocity regimes of flight or requires post-flight vehicle recovery for purposes of inspection or data recovery. Mitigation of this phenomena would also be required for Martian flight of this system without the use of parachutes or other decelerators. To achieve vehicle stability, a simple cold-gas attitude control system is proposed. The layout of the attitude control system is shown in figure 8 and its properties are listed in table 2. Four independent thrusters are placed at the aft end of the vehicle in pairs. Each thruster in a pair face the opposite direction of their partner. By simulataneously firing two thrusters pointed in the same direction, the controller can apply a positive or negative pitch torque to the vehicle. Since the dynamic instability severity is a function of the overall $\frac{\partial \alpha}{\partial s}$ term, by driving $\frac{\partial \alpha}{\partial s}$ to a small value we can mitigate the strength of the instability. To accomplish this, a simple pitch body-rate dead-band control law was implemented.

Table 2. Attitude Control System Properties

Thruster	Position*		Nozzle Direction†
1	$[0, 2, 0]$	m	$[0, 0, 1]$
2	$[0, -2, 0]$	m	$[0, 0, 1]$
3	$[0, -2, 0]$	m	$[0, 0, -1]$
4	$[0, 2, 0]$	m	$[0, 0, -1]$
Mean Thruster Force	300	N	

* Position is relative to origin in body coordinate system.
† Nozzle direction is expressed in the body coordinate system.

The control law simply actuates the appropriate thruster pair when the pitch axis body-rate magnitude exceeds a set value. For this study, a pitch rate limit of 5 deg/s was found to give the best performance in terms of propellant utilization while also being large enough not to be adversely affected by controller

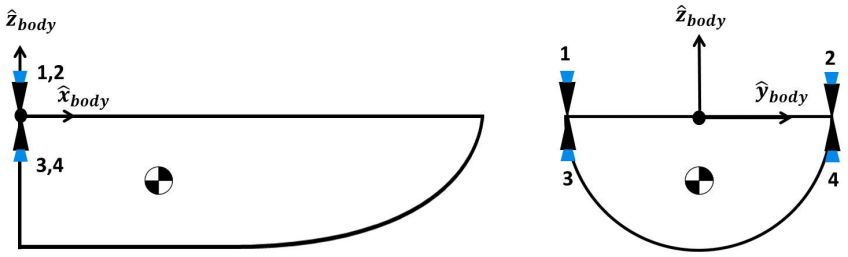

Figure 8. A simple cold-gas attitude control system was added to the vehicle to improve pitch stability.

lag and valve actuation delay. Utilizing the same initial conditions as the uncontrolled trajectory shown in figure 6, an actively controlled trajectory implementing the pitch body-rate dead-band control law is shown in figure 9. The control law successfully mitigates the dynamic instability and maintains vehicle stability around the static trim condition through the entirety of the descent.

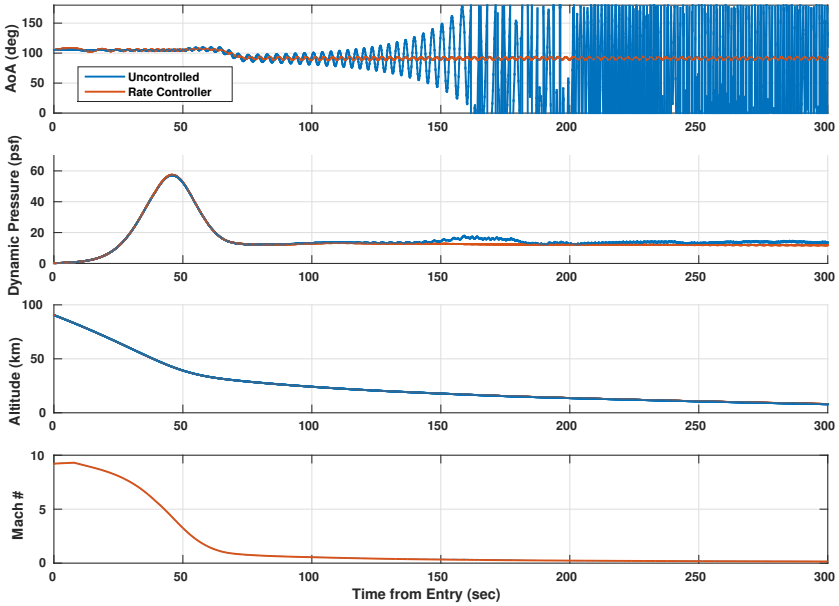

Figure 9. By implementing a body-rate dead-band control law, the attitude control system is able to maintain stability.

V. Conclusion

The Earth based entry performance of a half-ogive aeroshell was investigated. Six degree-of-freedom trajectory simulations show that the vehicle experiences benign entry environments at supersonic speeds largely because of its low ballistic coefficient. At subsonic speeds, a dynamic pitch instability was observed in simulation. The root cause of this instability was shown to be the change in lift with change in angle of attack. For the half-ogive aeroshell at high angles of attack, the lift vector works to push the angle of attack away from the aeroshell's trim condition. A method of mitigating this instability using a gaseous nitrogen attitude control system and a simple pitch rate control law was proposed and shown to effectively maintain vehicle stability during terminal descent.

References

[1]Bridges, J. C., Seabrook, A. M., Rothery, D. A., Kim, J. R., Pillinger, C. T., Sims, M. R., Golombek, M. P., Duxbury, T., Head, J. W., Haldemann, A. F. C., Mitchell, K. L., Muller, J.-P., Lewis, S. R., Moncrieff, C., Wright, I. P., Grady, M. M., and Morley, J. G., "Selection of the landing site in Isidis Planitia of Mars probe Beagle 2," *Journal of Geophysical Research: Planets*, Vol. 108, No. E1, 2003, pp. 1–1–1–17, 5001.

[2]Witkowski, A., Kandis, M., and Adams, D. S., "Mars Science Laboratory Parachute System Performance," *AIAA Aerodynamic Decelerator Systems (ADS) Conference*, American Institute of Aeronautics and Astronautics, 2016/04/30 2013.

[3]DwyerCianciolo, A. M., Davis, J. L., Komar, D. R., and Munk, M. M., "Entry, Descent and Landing Systems Analysis Study: Phase 1 Report," Tech. rep., NASA Langley Research Center, 2010.

[4]Clark, I. G., Manning, R., and Adler, M., "Summary of the First High-Altitude, Supersonic Flight Dynamics Test for the Low-Density Supersonic Decelerator Project," *23rd AIAA Aerodynamic Decelerator Systems Technology Conference*, American Institute of Aeronautics and Astronautics, 2016/04/30 2015.

[5]Hughes, S., Cheatwood, F., Dillman, R., Calomino, A., Wright, H., and DelCorso, J., "Hypersonic Inflatable Aerodynamic Decelerator (HIAD)Technology Development Overview," *21st AIAA Aerodynamic Decelerator Systems Technology Conference and Seminar*, American Institute of Aeronautics and Astronautics, 2016/04/30 2011.

[6]Giersch, L., Rivellini, T., Clark, I. G., Sandy, C., Sharpe, G., Shook, L. S., Ware, J. S., Welch, J., Mollura, J., and Dixon, M., "SIAD-R: A Supersonic Inflatable Aerodynamic Decelerator for Robotic missions to Mars," *AIAA Aerodynamic Decelerator Systems (ADS) Conference*, American Institute of Aeronautics and Astronautics, 2016/04/30 2013.

[7]Karatekin, Ö., *Aerodynamics of a Planetary Entry Capsule at Low Speeds*, Ph.D. thesis, Université Libre de Bruxelles, Belgium, 2001.